



Physical Characteristics of Low-Dose Nitrogen Ions-Implanted Copper Oxide Thin Film on n-Si (100) Substrate

Muhammad Arslan Ayub¹ · Naveed Afzal¹ · Mohsin Rafique¹ · Sameen Aslam^{2,3}

Received: 22 January 2024 / Accepted: 22 April 2024
© King Fahd University of Petroleum & Minerals 2024

Abstract

Thin film of copper oxide was deposited onto a silicon substrate through DC magnetron sputtering system. Nitrogen ions (N^+) were implanted into the film using Pelletron Accelerator at different doses (5×10^{12} , 5×10^{13} and 5×10^{14} ions/cm²) while maintaining a constant ion energy of 300 keV. The X-ray diffraction study revealed a diffraction peak of CuO (-111) in all the samples. The crystallite size of CuO decreased at 5×10^{12} ions/cm² and then increased with the dose up to 5×10^{14} ions/cm². The decrease in crystallite size was attributed to structural disorder in the film caused by ions irradiation, while at relatively higher doses ($> 5 \times 10^{12}$ ions/cm²), localized thermal effects improved the structural ordering of the material through the annihilation of defects. The surface morphology of the film showed a decrease in its grain size at 5×10^{12} ions/cm², followed by an increase with a further increase in the ion dose. N^+ implantation at 5×10^{12} ions/cm² decreased the surface roughness of CuO, while the roughness remained constant at the higher doses. The electrical resistivity of CuO decreased upon N^+ implantation at 5×10^{12} ions/cm² and then increased with a further increase in the ion dose. The band gap of the CuO exhibited a similar trend to that of its resistivity and crystallite size. These findings show that the N^+ implantation serves as an effective method for tuning the physical properties of the copper oxide film, for its superior performance in the electronic and optoelectronic devices.

Keywords CuO film · Sputtering · Nitrogen ions · Band gap · Resistivity · Morphology

1 Introduction

Copper oxide is a well-known semiconductor with p-type characteristics. It commonly exists in three primary phases, known as CuO (tenorite), Cu₂O (cuprite) and Cu₄O₃ (paramelaconite). Among these phases, the most stable forms of copper oxide are the tenorite and cuprite [1, 2]. Copper oxide exhibits a high absorption coefficient in visible region, along with high carrier mobility, and a wide band gap. As a result, copper oxide films are widely used in various devices including solar cells, gas

sensors, photo-electrochemical cells, photocatalysis, light emitting diodes, magnetic media, superconductors, antibacterial agent and photodetectors [3–13]. Copper oxide films can be synthesized using various methods, including both chemical/physical deposition techniques [14–18]. Among these methods, the magnetron-sputtered films exhibit superior uniformity and better adhesion to the substrate [19, 20]. Tuning the physical properties of metal oxides films through ion implantation is recognized as a valuable technique. In this process, impurity ions are introduced into metal oxides using an ion implanter or accelerator. The implanted ions can potentially enhance their physical properties. The controllability and repeatability of the results in the case of ions-implanted films are found to be superior to that of the chemically doped films [20–22]. Consequently, ion implantation in thin films is widely utilized to control and enhance their properties. Researchers have investigated the ion implantation effects in copper oxide film. Ahmad et al. [23] reported silver ion (Ag^+) implantation effects on the copper oxide film. The result revealed a decrease in refractive index, band gap, and resistivity of the film due to Ag^+ implantation. Ungeheuer

✉ Naveed Afzal
naveedafzal@gcu.edu.pk

¹ Centre for Advanced Studies in Physics, Government College University, Lahore, Pakistan

² School of Physics, Universiti Sains Malaysia, Penang, Malaysia

³ Department of Physics, Balochistan University of Information Technology, Engineering and Management Sciences, Quetta 87300, Pakistan



et al. [24] implanted chromium ions (Cr^+) at 10 keV into the magnetron-sputtered Cu_2O film at different doses. The Cr^+ implantation led to a reduction in optical absorption and an increase in the band gap of the film. Jafari et al. [25] investigated the copper oxide film's properties after implanting 30 keV nitrogen ions with a dose of 1×10^{18} ions/ cm^2 . The results indicated a decrease in grain size, an increase in surface roughness and band gap of the ion-implanted film. Similarly, Sberna et al. [26] reported a decrease in the electrical resistivity of the CuO film due to 46 keV N^+ implantation in it at different doses. Another study revealed that the 50 keV N^+ implantation enhanced the crystallinity of copper oxide while simultaneously reducing its sheet resistance [27]. All of these studies demonstrated a pivotal role of nitrogen ion implantation in controlling the physical properties of the copper oxide films.

The previous studies on nitrogen-implanted copper oxide films were mostly conducted using low-energy (< 100 keV) and high-dose nitrogen ions ($> 10^{15}$ ions/ cm^2). Low-energy ion implantation in a material leads to nuclear stopping, resulting in the creation of displacement cascades and lattice defects in the material [20]. In the present work, we employed relatively high-energy (300 keV) and low-dose (10^{12} – 10^{14} ions/ cm^2) nitrogen ions compared to the previous investigations. Here, the structural, electrical and optical properties of the N^+ -implanted copper oxide film have been examined at different doses.

2 Experimental Work

Thin films of copper oxide were deposited on n-type Si (100) substrates. The experiment was started with the cutting and cleaning of Si specimens of dimensions 1.5×1.5 cm^2 . The specimens were cleaned using acetone. A magnetron sputtering system comprising of a sputtering chamber, power supply and vacuum system was utilized for the deposition of copper oxide film. A copper target of purity 99.999% was cleaned using emery paper to eliminate any impurities on its surface before being placed inside the chamber. The pump was activated to create a vacuum in the chamber. Argon gas was introduced into the chamber along with oxygen ($\text{Ar}:\text{O}_2$ 80:20) to facilitate the reactive sputtering process. Plasma was generated by applying a DC voltage across the target and substrate. The initial and working pressures were measured to be 1×10^{-1} mbar and 0.002 mbar, respectively. Copper sputtering was conducted at 100 W with a deposition rate of 0.7 Å/sec [28]. The thickness of the CuO film was measured to be about 350 nm. Subsequently, deposited films on Si (100) were taken out of the chamber for ion implantation. One specimen was left pristine, while the others were implanted with nitrogen ions (N^+) using a Pelletron Accelerator (Model: 6SDH-2 NEC, USA). The operation of Pelletron Accelerator

is elucidated in our recent studies [20, 29]. To conduct ion implantation, the films were affixed to a plate inside the accelerator chamber. Nitrogen ions (N^+) were generated using a TiN SNICS cathode and were accelerated toward the films. The films were implanted with nitrogen ions at the doses of 5×10^{12} , 5×10^{13} and 5×10^{14} ions/ cm^2 , while the ion energy was same (300 keV) for all the specimens. The ion irradiation experiment was performed at room temperature. The SRIM software was utilized to determine the range of N^+ within the copper oxide film. Figure 1a, b displays the SRIM results of a copper oxide film implanted with 300 keV N^+ at a dose of 5×10^{14} ions/ cm^2 . The penetration range of N^+ within the film was determined to be 116 nm (Fig. 1a). Figure 1b presents the SRIM results of target displacements and vacancies induced by N^+ in the film.

X-ray diffraction analysis of pristine (untreated) and N^+ -implanted copper oxide was conducted using an x-ray PANalytical X'Pert Pro Diffractometer, employing $\text{Cu-}k$ -alpha radiations (step size = 0.02°) at 40 kV and 20 mA. The films were examined for surface morphology using a field emission scanning electron microscope (FESEM, Model: Nova NanoSEM 450). Morphological images were then utilized to generate topographic histograms through WSxM 5.0 develop Nanotech software for the measurement of surface roughness. Electrical resistivity of the films was measured using a four-probe apparatus, while the energy band gap was evaluated using ultraviolet–visible reflectance spectroscopy. The results obtained from these characterizations were subsequently correlated.

3 Results and Discussion

3.1 X-ray Diffraction Analysis

The X-ray diffraction (XRD) patterns of the copper oxide films are depicted in Fig. 2. Figure 2 reveals the presence of cupric oxide (CuO) phase of the film at 35.5° corresponds to (-111) plane, indicating monoclinic crystal structure (JCPDS Card No. 00-048-1548) [30]. No peaks related to Cu_2O and Cu_4O_3 phases were detected in the XRD patterns. The XRD patterns also show that the position, intensity and width of the CuO peak vary with changes in the N^+ dose. For a more detailed analysis, the peak position (2θ) has been plotted against the N^+ dose (Fig. 3a). The peak shifts to higher angle of diffraction with an increase in the dose to 5×10^{13} ions/ cm^2 and then to lower angle at 5×10^{14} ions/ cm^2 . The shift to a higher angle indicates compressive stresses in the N^+ -implanted film. Conversely, tensile stresses are produced at the higher dose, resulting in a lower-angle peak shift. These compressive stresses originate from structural disorder due to N^+ implantation. Implanting N^+ in CuO at 5×10^{14} ions/ cm^2 enhances the crystallinity of the material as

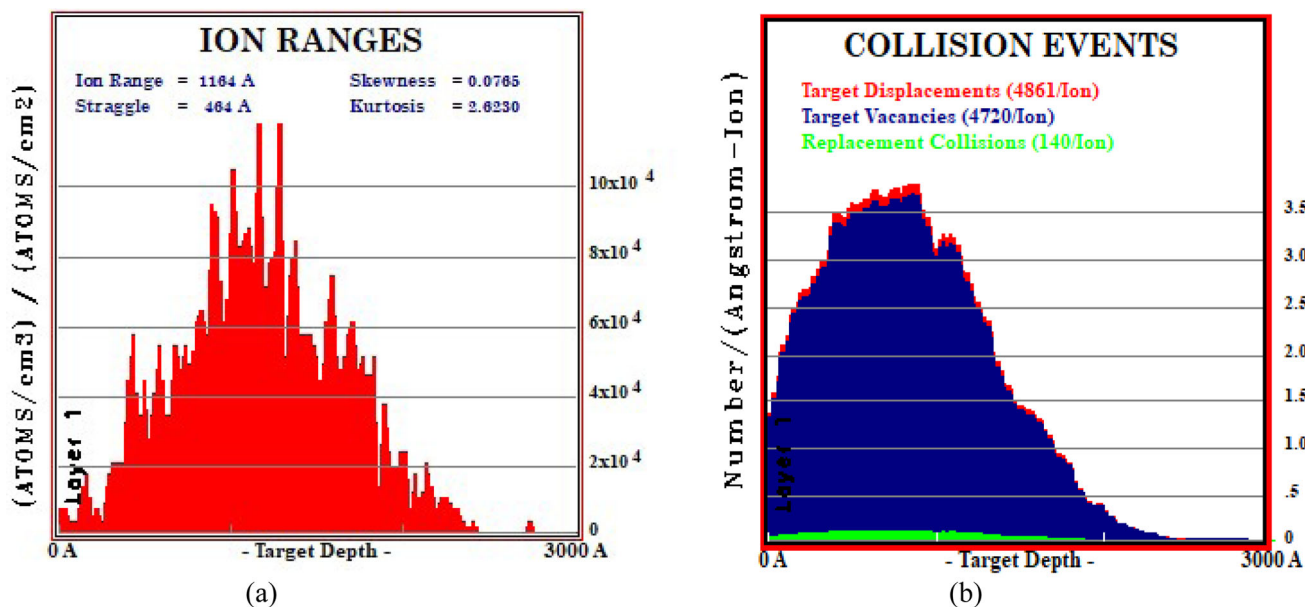


Fig. 1 a, b SRIM results of N⁺-implanted CuO film

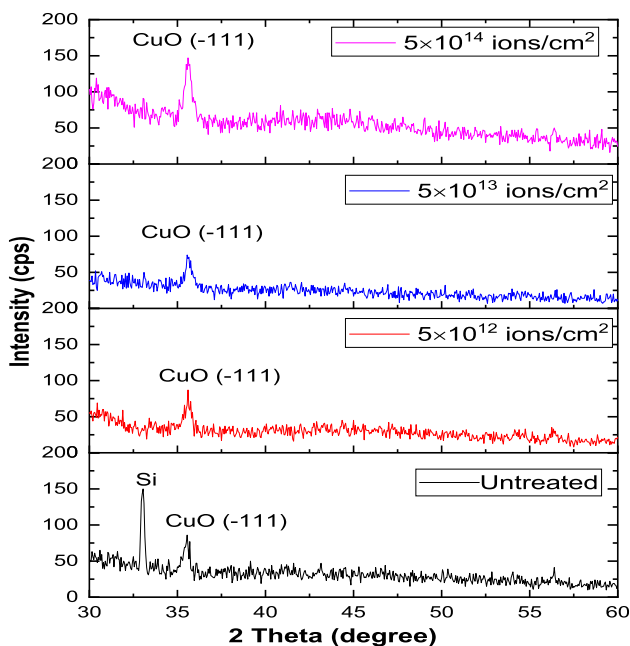


Fig. 2 XRD patterns of untreated and N⁺-implanted CuO films

N⁺ occupy the vacant oxygen sites. Since the oxygen ionic radius has a lower value (0.138 nm) than that of the nitrogen ionic radius (0.146 nm), this causes tensile stresses in the film [31].

Crystallite size (*D*), microstrain (ϵ) and dislocation density (δ) of the film were calculated using the following equations [32];

$$D = \frac{k\lambda}{\beta \cos \theta} \tag{1}$$

$$\epsilon = \frac{\beta \cot \theta}{4} \tag{2}$$

$$\delta = \frac{1}{D^2} \tag{3}$$

Here, *k* represents the shape constant, while the wavelength of X-rays, FWHM and Bragg’s angle are depicted here by λ , β and θ , respectively. Figure 3b illustrates the variations of *D* and ϵ of CuO with N⁺ dose, whereas Fig. 3c shows δ as a function of the N⁺ dose. The value of *D* decreased due to N⁺ implantation at 5×10^{12} ions/cm² and increased afterward at the higher N⁺ doses. The changes in ϵ and δ of the CuO film are found to be opposite to that of its crystallite size. In most of the previous studies, low-energy and high-dose nitrogen ion implantation in copper oxide films was investigated. For example, Jafri et al. [25] reported a decrease in the crystallite size ‘*D*’ of the Cu₂O-CuO film implanted with 30 keV nitrogen ions implantation at 1×10^{18} ions/cm². The decrease in the value of *D* was ascribed to high dislocations density and a large number of defects in the film. However, the results of Bind et al. [27] revealed the transformation of the amorphous copper oxide into crystalline Cu₂O phase by 50 keV nitrogen ion implantation at the lower dose (2.5×10^{15} ions/cm²) and the crystallinity of the Cu₂O was improved owing to the thermal effects of ion irradiation. By increasing the ion dose (1×10^{16} ions/cm²), the Cu₂O was converted into the CuO phase with a reduced value of *D*. In this work, 300 keV nitrogen ion implantation in CuO decreased its crystallinity at the lower dose, while at the higher doses ($> 5 \times 10^{12}$ ions/cm²),

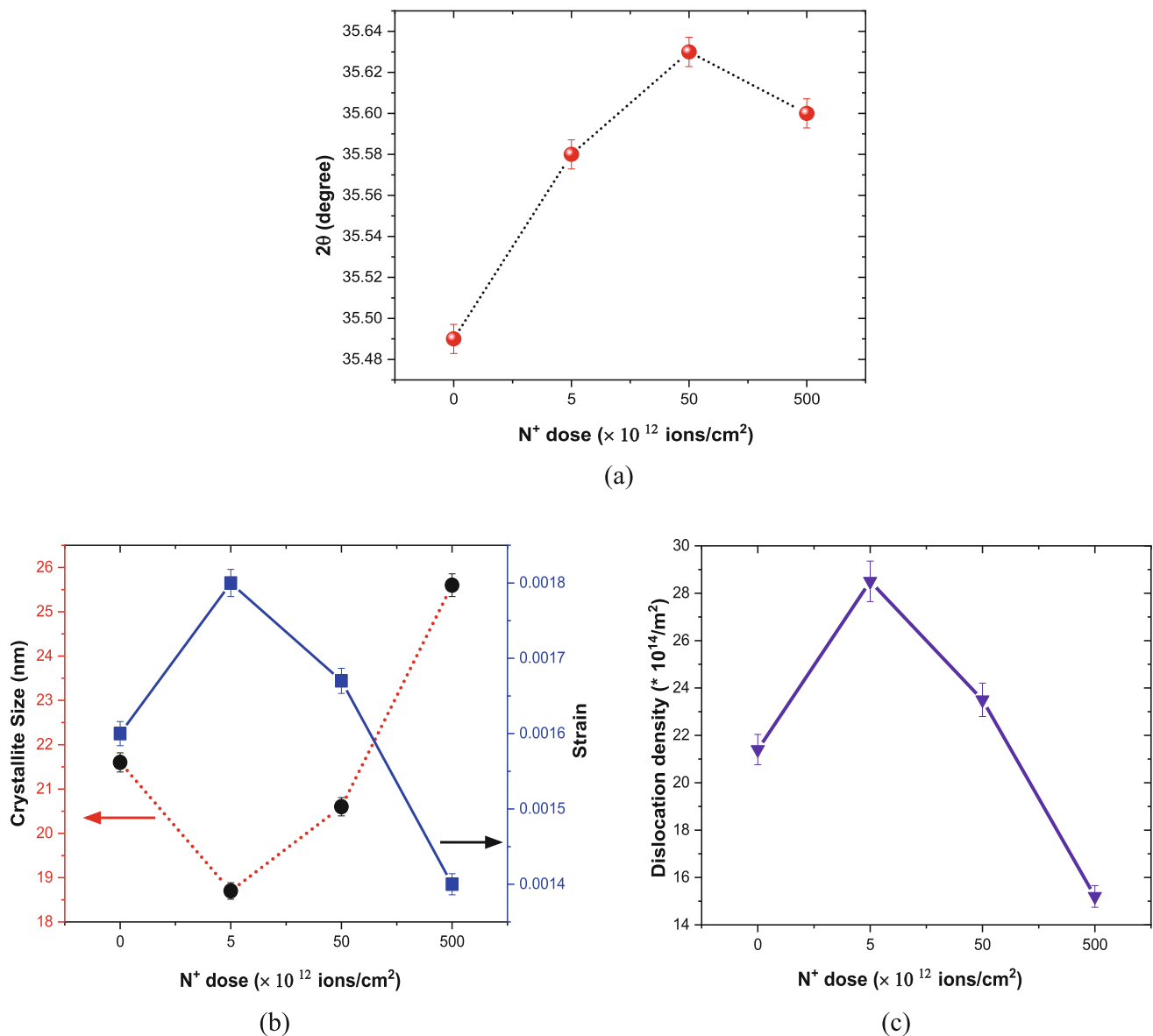


Fig. 3 a–c Variations of structural parameters of CuO film with N^+ dose

the crystallinity improved; however, no phase change was observed compared to the previous studies. The increase in crystallinity of a material is beneficial for improving the performance of electronic devices based on it. The structural properties of copper oxide film are explained here using a well-known model called the thermal-spike model of ion irradiation [20, 22, 29, 32, 33]. According to this model, ions interact with matter by colliding with its atoms either elastically or inelastically. The inelastic collisions occur when the ion and electron interactions take place, while the elastic collisions take place due to the ions–nuclei interactions. Both of these collisions result in creating radiation damage in the material through primary knock-on atoms formation and then displacement cascades. The energy lost by the atoms

during cascade collisions not only produces lattice disorder, but also produces localized heating in the material [32]. This heat minimizes the radiation damage through the annihilation of structural defects. The survived defects are responsible for changing the physical properties of the material. In this work, implanting 300 keV N^+ of dose 5×10^{12} ions/cm 2 , structural disorder in the film occurs due to the formation of vacancies and interstitials which decrease ‘D’ and increase ϵ and δ values of the film [20–22]. Increasing the ion dose to 5×10^{13} ions/cm 2 and above results in an increase in the number of incident ions on the material’s surface, causing more cascade collisions. This generates more localized heat in the surrounding area which minimizes the structural disorder of

the film. Consequently, the value of ‘*D*’ increased, whereas ‘*ε*’ and ‘*δ*’ decreased at the higher doses.

3.2 Surface morphology

The micrographs of CuO films (Mag. 200,000×) are presented in Fig. 4. These micrographs depict granular structure of the CuO. The grains are coarse and closely spaced together in the case of untreated film. These are randomly distributed with some grains agglomerated with each other. The grain boundaries are quite distinct in all the samples. The grain size of the film was calculated using ImageJ software. After irradiation at the lower ion dose of 5×10^{12} ions/cm², the number of grain boundaries increased, while with increasing ion dose, the size of grains increased, resulting in a reduction of grain boundaries.

Figure 5 shows the variation in grain size of CuO with respect to ion dose. The N⁺ implantation of CuO reduced the grain size at the lower dose (5×10^{12} ions/cm²) owing to ion-induced structural damage in the film, forming vacancies and interstitials [34]. As the dose was further increased, the grain size increased due to localized heating of the film by N⁺ implantation. This reduced the defects created during the elastic and inelastic collisions of ions with the CuO film, leading to an increase in the grain size. The surface morphology results validate the XRD results as discussed above. Similar types of radiation effects were reported in previous studies for ZnO films implanted with copper and nickel ions [20, 21].

3.3 Surface Roughness Study

Surface roughness of the untreated and N⁺-implanted CuO films was analyzed from the topographic histograms. The histograms (not shown here) were generated by WSxM 5.0 develop Nanotech software using morphological images that are depicted in Fig. 3. The root mean square value of the surface roughness was calculated by the following expression [35, 36]:

$$R = \left[\left(\frac{1}{N} \right) \sum_{i=1}^N (Z_i - Z_o)^2 \right]^{1/2} \tag{4}$$

Z_i is the value of a given specimen point obtained from the histograms, while *Z_o* is the average value of the specimen points in the analyzed area; thus, *Z_i* – *Z_o* is the absolute value of the surface profile deviation value from the mean line. The surface roughness was directly determined using WSxM 5.0 develop Nanotech software. The detail of the surface roughness calculation using this method has been elaborated in the literature [35, 36]. The surface roughness was plotted against the ion dose (Fig. 6). The roughness decreased due to N⁺

implantation at 5×10^{12} ions/cm² and then almost remained constant at the higher doses. The decrease in surface roughness is attributed to changes in the shape and size of the grains. When the N⁺ impinge on the surface of the CuO film, their energy is transferred to the target, resulting in structural disorder as well as simultaneously recovery due to excessive localized heat. The stresses within the grains are relaxed and the grains of the film arrange themselves in a regular form. This provides sufficient time for the atoms to resettle in the localized heat region. Consequently, the surface of the film becomes smooth and thus its roughness decreases. When the N⁺ dose increases, the roughness almost remains constant. Some previous studies have shown a change in the surface roughness of the copper oxide films due to ion implantation in their surface [24, 25, 27]. Jafari et al. demonstrated that 30 keV nitrogen ions implanted in the Cu₂O-CuO film at 1×10^{18} ions/cm² increased the surface roughness of the film due to enhanced atomic movement induced by the ion implantation [25]. In another study related to the low-energy nitrogen ion implantation in copper oxide film at higher doses (1×10^{16} ions/cm²), an increase in the surface roughness of the film was ascribed to the transformation of the Cu₂O into CuO phase [27].

3.4 Electrical Resistivity

Electrical resistivity is an important parameter that determines the electrical characteristics of a film. In this work, the four-probe method was used to measure current (*I*) and voltage (*V*) values of the CuO films, and the following equation was used to evaluate the electrical resistivity (*ρ*) of the film [21, 22, 37];

$$\rho = \left(\frac{\pi}{\ln 2} \right) \left(\frac{V}{I} \right) t \tag{5}$$

$\frac{\pi}{\ln 2}$ is the correction factor, and film thickness is represented by ‘*t*’ (350 nm). The electrical resistivity values of the untreated and N⁺-implanted CuO film are plotted against the ion dose (Fig. 7). For the untreated specimen, the electrical resistivity was 41.30 Ω-cm, which decreased to 5.42 Ω-cm upon ion implanting the nitrogen ions (with a dose of 5×10^{12} ions/cm²). The decrease in the electrical resistivity occurred due to the decrease in the crystallite size (*D*) of the material. The resistivity almost remained constant (7.98 Ω-cm) at 5×10^{13} ions/cm², while at a dose of 5×10^{14} ions/cm², the resistivity increased to 20.98 Ω-cm. The reduced resistivity due to N⁺ implantation occurs because of disruption in the structural order of the film. The formation of copper interstitials or oxygen vacancies in the film leads to a partial decrease in the semiconducting behavior of the CuO film [22]. On the contrary, the increase at the higher dose might be due to thermal recovery of the film due to localized rise in the

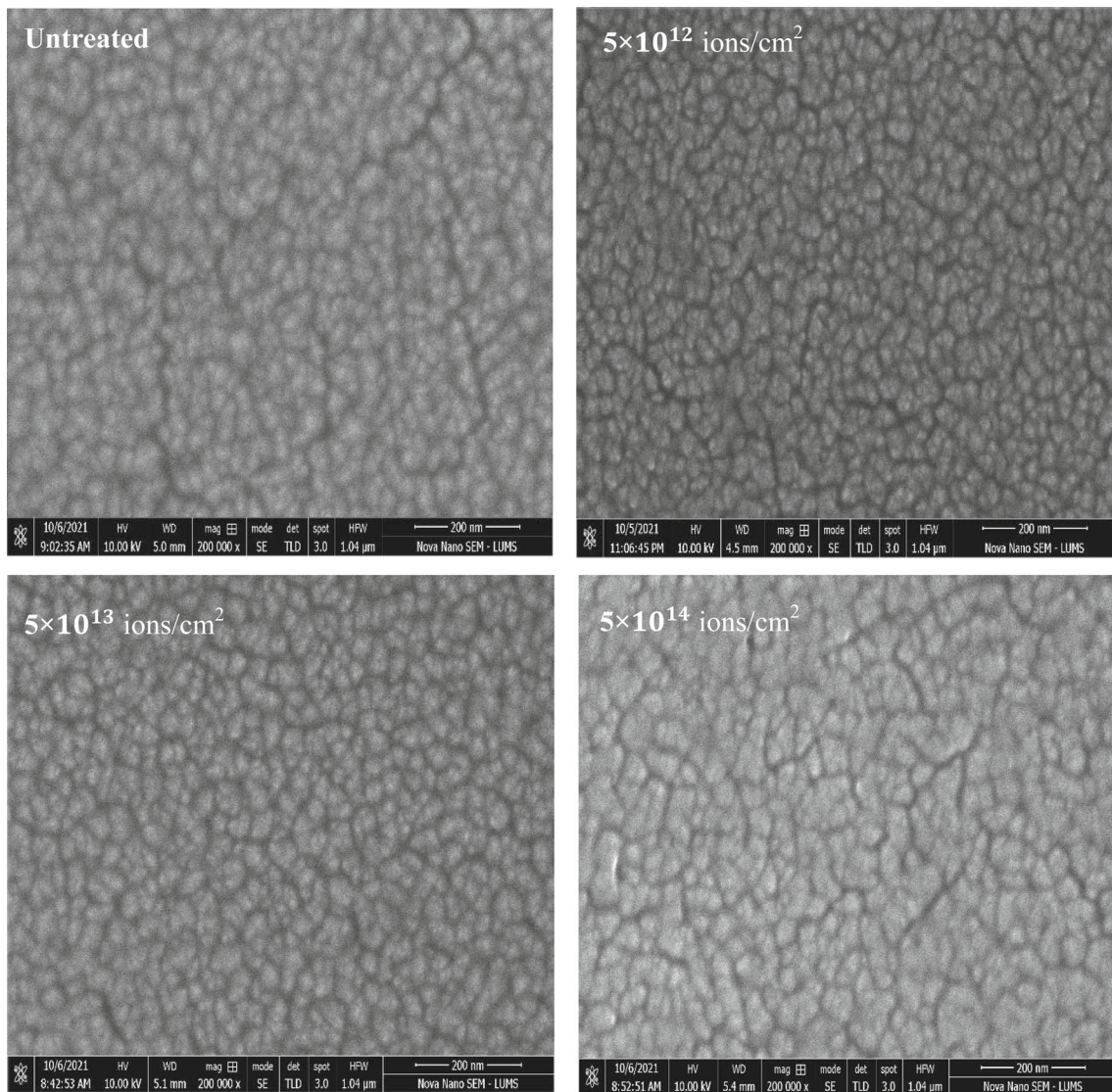


Fig. 4 Surface morphology of untreated and N^+ -implanted CuO films

temperature of the CuO lattice. Due to the decrease in the electrical resistivity, the electrical conductivity of the CuO film increases and vice versa. An increase in the N^+ dose results in more nitrogen ions being implanted into the CuO film, inducing collisional cascades in the material. Consequently, more heat is generated, which increases the film's resistivity at 5×10^{14} ions/cm². These results are consistent with the literature where the resistivity of the nitrogen ions-implanted Cu₂O film was decreased as compared to the untreated specimen [26, 27]. Additionally, these results can also be compared with another study, which indicates the dependence of the grain size of Gd–Ba–Cu–O with conducting copper oxide on its electrical resistivity [38].

3.5 Band Gap Analysis

The reflectance spectra of the untreated and N^+ -implanted films were obtained using a UV–vis spectrometer, and the data were analyzed. Figure 8a shows the results of the UV–vis spectra of the CuO film that contain interference fringes. The formation of these fringes is due to reflection of light beams from the substrate surface and the CuO film. A stage comes when these fringes disappear and the reflectance becomes almost constant. This occurs when the film starts absorbing the light and hence no more interference of the reflected beams occurs. The wavelength value at this stage is known as the cut-off wavelength (λ).

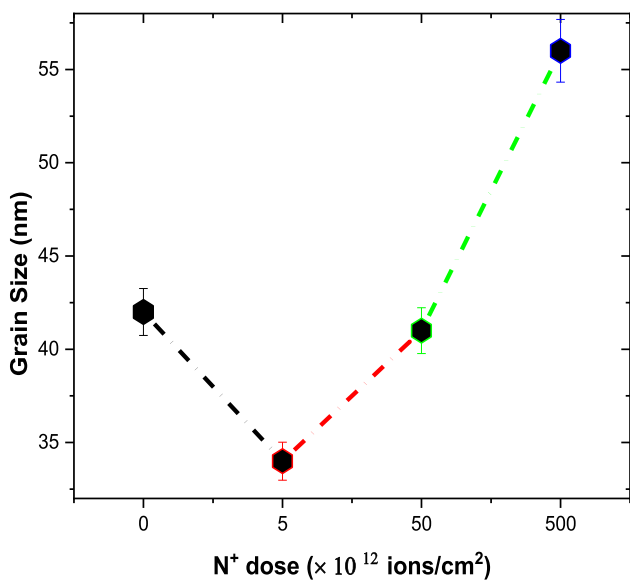


Fig. 5 Grain size variation of CuO film at different N⁺ doses

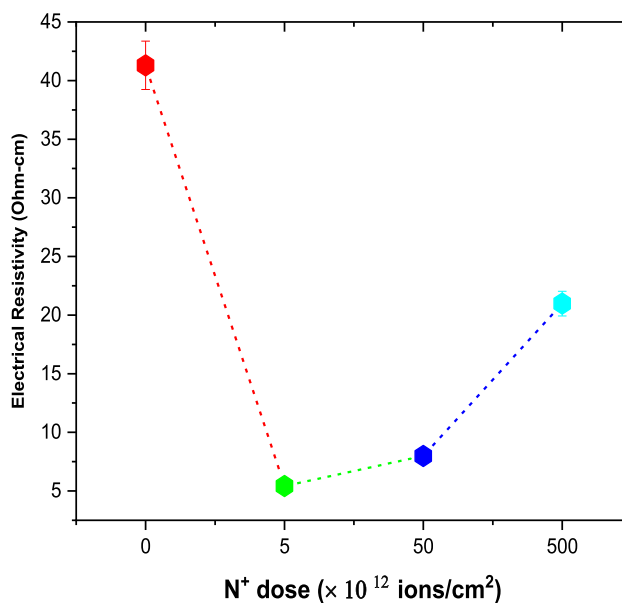


Fig. 7 Electrical resistivity of CuO film versus N⁺ dose

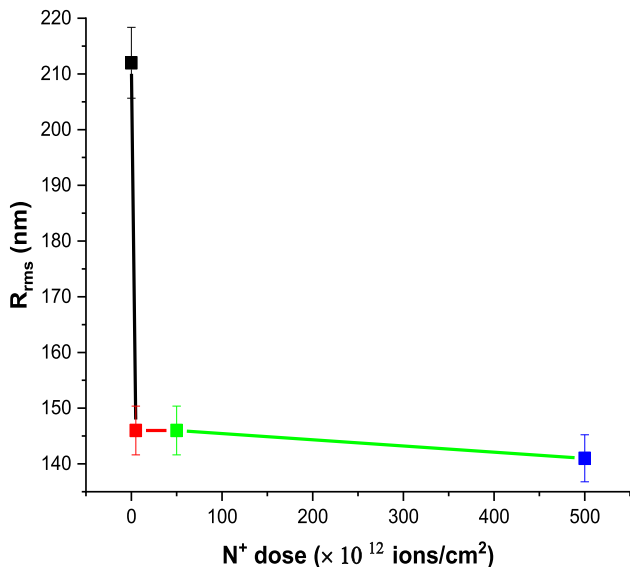


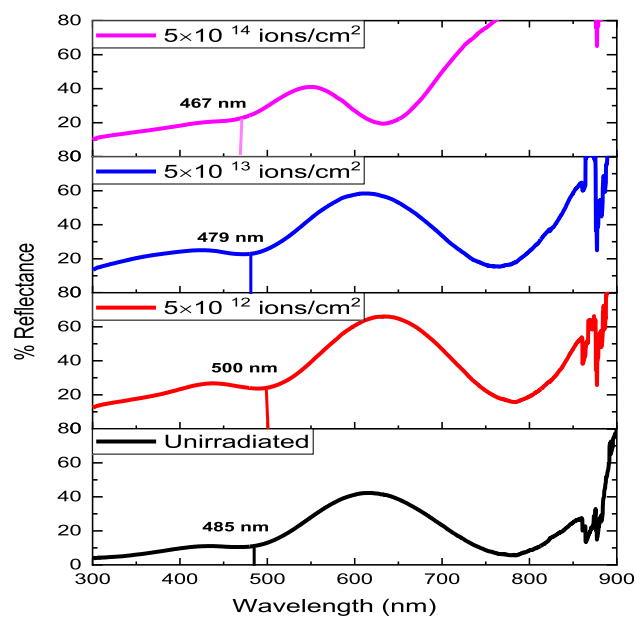
Fig. 6 Variation of surface roughness of CuO film with N⁺ dose

For finding the band gap energy (E_g) of the CuO film, the following relation was used [39, 40]:

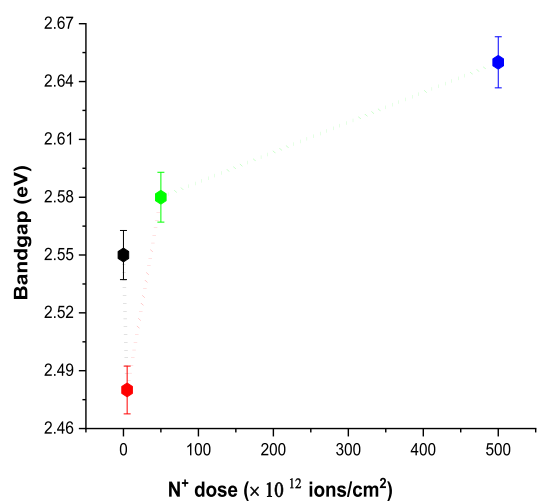
$$E_g = \frac{hc}{\lambda} \tag{6}$$

' h ' is the Planck's constant and ' c ' is the speed of light. The band gap was plotted against ion dose (Fig. 8b). The band gap decreased initially at the lower N⁺ dose (5×10^{12} ions/cm²) and then increased afterward. The high value of the band gap of copper oxide is attributed to the quantum size effect [11, 28]. These results show that changes in the band gap

of CuO are similar to those noticed in the electrical resistivity and grain size of the film. A decrease in the grain size causes a decrease in both the resistivity and the band gap of the CuO film and vice versa. This effect is more pronounced at the lower ion dose due to lattice disorder. As a result, the semiconducting nature of the CuO partially exhibits metallic character. However, implanting N⁺ in CuO at higher dose results in the improvement of film's crystallinity, owing to the localized rise of temperature. This increases the electrical resistivity and facilitates the widening of the CuO band gap. The high band gap of CuO permits the absorption of lower wavelength light and vice versa. Therefore, tuning the band gap of copper oxide is helpful in enhancing the performance of the devices based on it. Different observations have been made regarding the change in the band gap of the copper oxide film due to ion implantation. The work of Jafari et al. [25] reported an increase in the band gap of nitrogen-implanted Cu₂O film due to the quantum size effect. Sberana et al. [26] demonstrated that the nitrogen ion implantation in the Cu₂O film reduces its band gap due to decrease in the oxygen vacancies, whereas, in this work, the band gap changes are associated with the changes in the structural and surface features of the film. The results obtained here show that the low-dose nitrogen implantation in copper film is equally effective in tuning its optical and electrical properties as previously done by the use of high-dose and low-energy nitrogen ion implantation.



(a)



(b)

Fig. 8 **a** UV–Vis reflectance spectra of untreated and N^+ -implanted CuO films. **b** Variation of energy band gap of CuO film with N^+ dose

4 Conclusions

The implantation of nitrogen ions (N^+) at an energy of 300 keV in copper oxide film induces structural defects in it at lower dose (5×10^{12} ions/cm²), leading to a reduction in the crystallite size/grain size. However, at higher doses ($> 5 \times 10^{12}$ ions/cm²), the effects of localized heating reduce structural defects, resulting in an increase in the crystallite size and grain size of the film. Furthermore, N^+ implantation in CuO results in a smoother surface compared to the untreated specimen, attributed to changes in the shape, size

and orientation of the film's grains. Moreover, at lower dose (5×10^{12} ions/cm²), N^+ implantation decreases resistivity and band gap of the CuO film. The results presented here demonstrate that optimizing the electrical and optical properties of CuO has the potential to improve its performance in electronic and optoelectronic devices. For future investigations, exploring the effects of implanting various other types of ions in the copper oxide film could further refine its properties.

References

- Serin, N.; Serin, T.; Horzum, S.; Celik, Y.: Annealing effects on the properties of copper oxide thin films prepared by chemical deposition. *Semicond. Sci. Technol.* **20**, 398–401 (2005)
- Murali, D.S.; Aryasomayajula, S.: Thermal conversion of Cu_4O_3 into CuO and Cu_2O and the electrical properties of magnetron sputtered Cu_4O_3 thin films. *Appl. Phys. A* **124**, 1–7 (2018)
- Jayatissa, A.H.; Guo, K.; Jayasuriya, A.C.: Fabrication of cuprous and cupric oxide thin films by heat treatment. *Appl. Surf. Sci.* **255**(23), 9474–9479 (2009)
- Wong, T.K.; Zhuk, S.; Masudy-Panah, S.; Dalapati, G.K.: Current status and future prospects of copper oxide heterojunction solar cells. *Materials* **9**(4), 271 (2016)
- Steinhauer, S.: Gas sensors based on copper oxide nanomaterials: a review. *Chemosensors* **9**(3), 51 (2021)
- Hubička, Z.; Zlámál, M.; Čada, M.; Kment, Š; Krýsa, J.: Photoelectrochemical stability of copper oxide photocathodes deposited by reactive high power impulse magnetron sputtering. *Catal. Today* **328**, 29–34 (2019)
- Baran, T.; Visibile, A.; Busch, M.; He, X.; Wojtyła, S.; Rondinini, S.; Minguzzi, A.; Vertova, A.: Copper oxide-based photocatalysts and photocathodes: fundamentals and recent advances. *Molecules* **26**(23), 7271 (2021)
- Zhoua, Y.; Li, J.; Peng, W.; Liu, Y.; Zhang, J.; Xiang, G.; Zhu, X.; Li, R.; Wang, H.; Deng, G.; Zhao, Y.: Near-white light-emitting diode from p-CuO/n-GaN heterojunction with an i-CuO electron blocking layer. *J. Alloy. Compd.* **867**, 159145–1–159148 (2021)
- Sagadevan, S.; Vennila, S.; Marlinda, A.R.; Al-Douri, Y.; Rafie Johan, M.; Anita Lett, J.: Synthesis and evaluation of the structural, optical, and antibacterial properties of copper oxide nanoparticles. *Appl. Phys. A* **125**, 1–9 (2019)
- Song, H.J.; Seo, M.H.; Choi, K.W.; Jo, M.S.; Yoo, J.Y.; Yoon, J.B.: High-performance copper oxide visible-light photodetector via grain-structure model. *Sci. Rep.* **9**(1), 7334 (2019)
- Tariq, M.; Afzal, N.; Rafique, M.: Enhanced photodetection performance of sputtered cupric oxide thin film through annealing process. *Opt. Quantum Electron.* **53**, 1–16 (2021)
- Kutuk, S.; Bolat, S.; Terzioglu, C.; Altintas, S.P.: An investigation of magnetoresistivity properties of an $Y_3Ba_5Cu_8O_y$ bulk superconductor. *J. Alloy. Compd.* **650**, 159–164 (2015)
- Bolat, S.; Kutuk, S.: Fabrication of the new $Y_3Ba_5Cu_8O_y$ superconductor using melt–powder–melt–growth method and comparison with $YBa_2Cu_3O_{7-x}$. *J. Superconduct. Magn.* **25**, 731–738 (2012)
- Osorio-Rivera, D.; Torres-Delgado, G.; Márquez-Marín, J.; Castaneda-Pérez, R.; Aguilar-Frutis, M.A.; Zelaya-Ángel, O.: Cuprous oxide thin films obtained by spray-pyrolysis technique. *J. Mater. Sci. Mater. Electron.* **29**, 851–857 (2018)
- Figueiredo, V.; Elangovan, E.; Goncalves, G.; Barquinha, P.; Pereira, L.; Franco, N.; Alves, E.; Martins, R.; Fortunato, E.: Effect of post-annealing on the properties of copper oxide thin films



- obtained from the oxidation of evaporated metallic copper. *Appl. Surf. Sci.* **254**, 3949–3954 (2008)
16. Farhad, S.F.U.; Webster, R.F.; Cherns, D.: Electron microscopy and diffraction studies of pulsed laser deposited cuprous oxide thin films grown at low Substrate temperatures. *Materialia* **3**, 230–238 (2018)
 17. Shukor, A.H.; Alhattab, H.A.; Takano, I.: Electrical and optical properties of copper oxide thin films prepared by DC magnetron sputtering. *J. Vac. Sci. Technol. B* **38**, 012803-1–12805 (2020)
 18. Tadjine, R.; Houimi, A.; Alim, M.M.; Oudini, N.: Oxygen flow rate effect on copper oxide thin films deposited by radio frequency magnetron sputtering. *Thin Solid Films* **741**, 139013 (2022)
 19. Ahmad, H.; Afzal, N.; Rafique, M.; Ahmed, A.A.; Ahmad, R.; Khaliq, Z.: Post-deposition annealed MoO₃ film based high performance MSM UV photodetector fabricated on Si (100). *Ceram. Int.* **46**, 20477–20487 (2020)
 20. Imran, M.; Ahmad, R.; Afzal, N.; Rafique, M.: Copper ion implantation effects in ZnO film deposited on flexible polymer by DC magnetron sputtering. *Vacuum* **165**, 72–80 (2019)
 21. Younas, R.; Afzal, N.; Rafique, M.; Imran, M.; Saleem, M.; Ahmad, R.: Nickel ion implantation effects on DC magnetron sputtered ZnO film prepared on Si (100). *Ceram. Int.* **45**, 15547–15555 (2019)
 22. Imran, M.; Ahmad, R.; Afzal, N.; Rafique, M.: Modification in ZnO film properties by 250 keV cobalt implantation. *Mater. Res. Express* **6**(12), 126428 (2020)
 23. Ahmad, R.; Anjum, F.; Gillani, S.S.A.; Iqbal, M.W.; Zafar, K.; Ikhlague, U.; Saleem, S.; Naeem, M.: Study the effect of silver ion implantation on the structural, optical, and electrical properties of copper oxide thin films: an experimental and theoretical approach. *Eur. Phys. J. Plus* **136**, 1–15 (2021)
 24. Ungeheuer, K.; Marszalek, K.W.; Mitura-Nowak, M.; Jelen, P.; Perzanowski, M.; Marszalek, M.; Sitarz, M.: Cuprous oxide thin films implanted with chromium ions—optical and physical properties studies. *Int. J. Mol. Sci.* **23**, 8358 (2022)
 25. Jafari, A.; Tahani, K.; Dastan, D.; Asgary, S.; Shi, Z.; Yin, X.-T.; Zhou, W.-D.; Garmestani, H.; Tãlu, Ș.: Ion implantation of copper oxide thin films; statistical and experimental results. *Surf. Interfaces* **18**, 100463 (2020)
 26. Sberna, P.M.; Crupi, I.; Moscatelli, F.; Privitera, V.; Simone, F.; Miritello, M.: Sputtered cuprous oxide thin films and nitrogen doping by ion implantation. *Thin Solid Films* **600**, 71–75 (2016)
 27. Bind, U.C.; Dutta, R.K.; Sekhon, G.K.; Yadav, K.L.; Krishna Ranjini Menon, J.B.M.; Nabhiraj, P.Y.: Ion implantation induced phase transformation and enhanced crystallinity of as deposited copper oxide thin films by pulsed laser deposition. *Superlattices Microstruct.* **84**, 24–35 (2015)
 28. Farrukh, S.; Afzal, N.; Ahmed, A.A.; Rafique, M.; Raza, M.A.: Fabrication and characterization of MSM photodetector based on DC sputtered CuO film. *J. Optoelectron. Adv. Mater.* **23**, 530–537 (2021)
 29. Khan, A.; Rafique, M.; Afzal, N.; Khaliq, Z.; Ahmad, R.: Structural characterization of Zircaloy-4 subjected to helium ions irradiation of variable fluence. *Nucl. Mater. Energy* **20**, 100690 (2019)
 30. Diachenko, O.; Kováč, J., Jr.; Dobrozhan, O.; Novák, P.; Kováč, J.; Skriniarova, J.; Opanasyuk, A.: Structural and optical properties of CuO thin films synthesized using spray pyrolysis method. *Coatings* **11**(11), 1392 (2021)
 31. Lee, Y.S.; Heo, J.; Winkler, M.T.; Siah, S.C.; Kim, S.B.; Gordon, R.G.; Buonassisi, T.: Nitrogen-doped cuprous oxide as a p-type hole transporting layer in thin-film solar cells. *J. Mater. Chem. A* **1**, 15416–15422 (2013)
 32. Imran, M.; Ahmad, R.; Afzal, N.; Rafique, M.; Raza, M.A.; Khaliq, Z.: Structural, optical and electrical characteristics of silver ions irradiated ZnO film on flexible substrate. *Superlattices Microstruct.* **144**, 106586 (2020)
 33. Kaleem, A.; Bashir, S.; Akram, M.; Amir, R.; Mahmood, K.; Rafique, M.S.; Naseem, S.; Riaz, S.; Sarwar, M.; Tariq, A.: Carbon ion irradiation effects on surface modifications and field emission properties of molybdenum. *Appl. Phys. A* **128**(7), 561 (2022)
 34. Afzal, N.; Rafique, M.; Abbasi, A.; Ahmad, R.; Saleem, M.; Lee, J.M.: Impact of variable energy hydrogen ions on structural and mechanical properties of Zircaloy-4. *Phys. Scripta* **93**(11), 115303 (2018)
 35. Maqsood, M.; Rafique, M.; Butt, M.Z.; Afzal, N.; Usman Tanveer, M.; Imran, M.; Farooq, A.: Impact of carbon ion implantation on the crystal structure, surface morphology, vickers hardness and electrochemical corrosion of zirconium. *J. Mater. Eng. Perform.* **30**, 4604–4618 (2021)
 36. Butt, M.Z.; Ali, D.; Usman Tanveer, M.; Naseem, S.: Surface roughness and electrical resistivity of high-purity zinc irradiated with nanosecond visible laser pulses. *Appl. Surf. Sci.* **305**, 466–473 (2014)
 37. Khan, M.F.; Siraj, K.; Sattar, A.; Faiz, H.; Usman, A.; Raisanen, J.: Modification of structural and electrical properties of ZnO thin films by Ni²⁺ ions irradiation. *Dig. J. Nanomater. Biostruct.* **12**, 689–695 (2017)
 38. Kutuk, S.; Bolat, S.: Analysis of structural, electrical, and levitation properties of (RE: Nd, Sm, Gd) BCO-358 superconducting ceramics prepared by a modified MPMG technique. *J. Mater. Sci.* **57**, 1198–1214 (2022)
 39. Ahmed, A.A.; Devarajan, M.; Afzal, N.: Effects of substrate temperature on the degradation of RF sputtered NiO properties. *Mater. Sci. Semicond. Process.* **63**, 137–141 (2017)
 40. Ahmed, A.A.; Afzal, N.; Devarajan, M.; Subramani, S.: Structural, morphological, optical and electrical properties of NiO films prepared on Si (100) and glass substrates at different thicknesses. *Mater. Res. Express* **3**(11), 116405 (2016)

Springer Nature or its licensor (e.g. a society or other partner) holds exclusive rights to this article under a publishing agreement with the author(s) or other rightsholder(s); author self-archiving of the accepted manuscript version of this article is solely governed by the terms of such publishing agreement and applicable law.

